BBA - Biomembranes 1862 (2020) 183257

Contents lists available at ScienceDirect

BBA - Biomembranes

journal homepage: www.elsevier.com/locate/bbamem

Active $S^{21}68$ and inactive S^{21}IRS pinholin interact differently with the lipid bilayer: A ^{31}P and ^{2}H solid state NMR study

Daniel L. Drew Jr[a], Brandon Butcher[a], Indra D. Sahu[a,b], Tanbir Ahammad[a], Gunjan Dixit[a], Gary A. Lorigan[a,*]

[a] Department of Chemistry and Biochemistry, Miami University, Oxford, OH 45056, USA
[b] Natural Science Division, Campbellsville University, Campbellsville, KY 42718, USA

ARTICLE INFO

Keywords:
Pinholin
Phage lysis
Protein-lipid interactions
Phospholipid bilayers
Solid-state NMR

ABSTRACT

Pinholins are a family of lytic membrane proteins responsible for the lysis of the cytosolic membrane in host cells of double stranded DNA bacteriophages. Protein-lipid interactions have been shown to influence membrane protein topology as well as its function. This work investigated the interactions of pinholin with the phospholipid bilayer while in active and inactive confirmations to elucidate the different interactions the two forms have with the bilayer. Pinholin incorporated into deuterated DMPC-d_{54} lipid bilayers, along with ^{31}P and ^{2}H solid state NMR (SS-NMR) spectroscopy were used to probe the protein-lipid interactions with the phosphorus head group at the surface of the bilayer while interactions with the ^{2}H nuclei were used to study the hydrophobic core. A comparison of the ^{31}P chemical shift anisotropy (CSA) values of the active $S^{21}68$ pinholin and inactive S^{21}IRS pinholin indicated stronger head group interactions for the pinholin in its active form when compared to that of the inactive form supporting the model of a partially externalized peripheral transmembrane domain (TMD) of the active $S^{21}68$ instead of complete externalized TMD1 as suggested by Ahammad et al. JPC B 2019. The ^{2}H quadrupolar splitting analysis showed a decrease in spectral width for both forms of the pinholin when compared to the empty bilayers at all temperatures. In this case the decrease in the spectral width of the inactive S^{21}IRS form of the pinholin showed stronger interactions with the acyl chains of the bilayer. The presence of the inactive form's additional TMD within the membrane was supported by the loss of peak resolution observed in the ^{2}H NMR spectra.

1. Introduction

The initial step of host cell lysis by double-stranded DNA bacteriophage is the permeabilization of the inner cytosolic membrane. This permeabilization initiates the activity of the muralytic endolysin enzyme to begin peptidoglycan degradation. This is accomplished by a family of membrane proteins known as holins [1,2]. There are many subfamilies of holins, the most well studied being the λ S105 canonical holin which has three transmembrane helices and forms a single micron-scale hole in the membrane [3–5]. This allows for the release fully folded and functional endolysin from the cytoplasm [6]. This study will focus on the less studied lambdoid bacteriophage Φ21 pinholin, named such due to the numerous nanometer-scale holes it forms throughout the membrane. Pinholin is composed of two amphipathic helical transmembrane domains and, due to a dual translational start motif in the S^{21} gene, is expressed as an active $S^{21}68$ pinholin and a $S^{21}71$ antipinholin [7,8]. This $S^{21}71$ antipinholin is the negative-dominant form of the pinholin and is responsible for slowing the timing of membrane lysis. The pinholin pathway begins with the harmless accumulation of both forms of the pinholin in the cytosolic membrane where nonfunctional $S^{21}68$ homodimers and $S^{21}68$:$S^{21}71$ heterodimers begin to form at a 2:1 ratio [9]. These dimers require the externalization of the first transmembrane helical domain (TMD1) from the membrane to become functional [10]. Due to the additional positively charged lysine found on the N-termini of the $S^{21}71$ antipinholin the externalization of TMD1 in this case is slowed which delays the triggering of host cell lysis. This may be since the externalization requires dragging the lysine through the membrane interior. Understanding the differences between these two forms of the pinholin and their interactions with the lipid bilayer will help to gain a better insight into the beginning steps of the bacteriophage lytic pathway. This biophysical work will probe the different protein-lipid interactions pinholin has

* Corresponding author: Department of Chemistry and Biochemistry, 651 E. High St., Oxford, OH 45056, USA.
E-mail addresses: drewdl@miamioh.edu (D.L. Drew), butchebj@miamioh.edu (B. Butcher), sahuid@miamioh.edu (I.D. Sahu), ahammat@miamioh.edu (T. Ahammad), dixitg@miamioh.edu (G. Dixit), gary.lorigan@miamioh.edu (G.A. Lorigan).

https://doi.org/10.1016/j.bbamem.2020.183257
Received 31 July 2019; Received in revised form 28 February 2020; Accepted 2 March 2020
Available online 05 March 2020

with the membrane bilayer while in the inactive conformation, before TMD1 externalization, and in the active conformation with TMD1 externalized. This system will be studied utilizing ^{31}P and ^{2}H solid state nuclear magnetic resonance (SS-NMR) spectroscopy.

SS-NMR spectroscopy is a powerful biophysical technique that has been widely used to study the structure, topology, and dynamics of membrane proteins as well as their interactions with the lipid bilayer [11,12]. These protein-lipid interactions have been shown to be critical in several biological processes and have been known to impact the aggregation or segregation of proteins within the membrane, the overall function of the proteins, and the association of lytic proteins to the membrane [13–16]. Incorporation of proteins into synthetic phospholipid bilayers yields a more relevant biological simulation of protein-lipid interactions than monolayers or detergent micelles [17–19]. The effect of pinholin on the hydrophilic phospholipid headgroups and hydrophobic acyl chains of these bilayers can be probed through SS-NMR spectroscopy and incorporation of pinholin into deuterated DMPC (d_{54}-DMPC) liposomes. ^{31}P SS-NMR spectral line shapes are sensitive to the local environment around the ^{31}P head group and can give insight into the overall lipid dynamics within the system, and lipid phases. The ^{31}P nuclei of the phosphocholine headgroup of DMPC can reveal different dynamic effects between active and inactive pinholin at the surface of the membrane [20–22]. ^{2}H SS-NMR spectroscopy of deuterated lipid acyl chains can be used to obtain insight into the dynamics and chain order or packing of the acyl chains within the hydrophobic core of the membrane [20,23,24]. The use of both NMR active nuclei can be combined to determine the interactions of the pinholin with both the lipid head groups and the hydrophobic core of the membrane and how those interactions differ when the pinholin is in its active or inactive conformation. This study focuses on the different protein-lipid interactions between active and inactive pinholin with respect to TMD1's partial externalization from the membrane, the influence of the remaining TMDs on the packing of the acyl chains within the membrane, and the effects of both pinholin concentration and temperature changes on the properties of the DMPC lipid bilayer. This study also highlights the versatility and application of the biophysical technique SS-NMR to differentiate between two different conformations of the same protein.

2. Materials and methods

2.1. Solid phase peptide synthesis

All pinholin proteins were synthesized on a CEM Liberty Blue Solid Phase Peptide Synthesizer with a Discover Bio Microwave System. The solid phase was a NovaSyn TG amino resin, a composite of cross-linked polystyrene with the PEG chains terminally functionalized with the first amino acid group of the pinholin sequence. All Fmoc protected amino acids, as well as the activator diisopropylcarbodiimide (DIC), and activator base oxyma, were purchased from Millipore Sigma. Amino acid solutions were prepared at a 0.2 M concentration and coupled using DIC and oxyma at 90 °C for 4 min. Fmoc deprotection was run with 20% piperidine in dimethylformamide (DMF) at 93 °C for 1 min [25]. The resin and side chain protecting groups were cleaved from the protein using a 30 mL, three-hour trifluoroacetic acid (TFA) cleavage reaction, [94% TFA, 2.5% triisoproylsilane (TIPS), 2.5% 1,2-Ethanedithiol (EDT), 1% water] [26–28]. The TFA was evaporated off with a N_2 gas flow and the crude pinholin was precipitated from the remaining solution using tert-butyl methyl ether.

2.2. Protein purification

The crude pinholin peptide was purified using reverse phase high pressure liquid chromatography (RP-HPLC) on a C4 column and was eluted using a two-solvent gradient. The first solvent was deionized water, the second was 90% HPLC grade acetonitrile. Both solvents were degassed and then acidified with 0.1% TFA by volume. The pinholin protein was collected in fractions and the molecular weight of the protein was confirmed using Matrix Assisted Laser Desorption Ionization – Time of Flight Spectrometry (MALDI-TOF) [28]. Collected fractions were dried using lyophilization to recover the purified pinholin. An illustrative example of the HPLC Chromatogram and MALDI-TOF mass spectrum of the inactive S^{21}IRS-WT is shown in Fig. S4 in the supporting information.

2.3. Proteoliposome sample preparation

The active S^{21}68 and inactive S^{21}IRS pinholin were incorporated into 1,2-Dimyristoyl – d_{54} – sn – Glycero – 3 – Phosphocholine (DMPC) multilamellar vesicles (MLV) which have been shown to be successful at mimicking a lipid bilayer for membrane protein studies [29,30]. DMPC-d_{54} was purchased from Avanti Polar Lipids. These MLVs were created by dissolving a known amount of pinholin in TFE and adding the protein to DMPC dissolved in chloroform at a protein concentration at either 1 mol% or 2 mol%. The solvents were evaporated off using inert N_2 gas and the remaining lipid/protein film was rehydrated using 4-(2-hydroxyethyl)-1-piperazineethanesulfonic acid (HEPES) buffer created with deuterium depleted water at a concentration of 10 mM and adjusted to a neutral pH of ~7.0. All samples were rehydrated with the HEPES buffer to a final lipid concentration of 50 mM. To improve incorporation and MLV formation the protein/lipid solution was flash frozen in liquid nitrogen and then sonicated. This freeze-thaw cycle was repeated 3 times.

2.4. Solid state nuclear magnetic resonance spectroscopy

The solid-state nuclear magnetic resonance spectroscopy measurements were conducted using a Bruker 500 MHz WB UltraShield NMR spectrometer with a 4 mm triple resonance CP-MAS probe. ^{31}P NMR spectra were recorded with ^{1}H decoupling using a 4 μs $\pi/2$ pulse and a 4 s recycle delay, a spectral width of 300 ppm, and by averaging 6 K scans. A 50 kHz radio frequency field strength was used for ^{1}H decoupling. The collected free induction decay was processed using 300 Hz of line broadening. ^{2}H NMR spectra were collected at 76.77 MHz using a standard quadrupolar echo pulse sequence (3 μs 90° pulse length, 40 μs inter-pulse delay with a 0.5 s recycle delay) [31]. The spectral width was set to 100 kHz and 80 K transients were averaged for every ^{2}H NMR spectra. Exponential line broadening of 100 Hz was applied to the free induction decay before the Fourier transformation was taken. Both ^{31}P and ^{2}H SS-NMR experiments were collected from 25 °C to 55 °C in 10 °C increments and the sample was left to equilibrate to each temperature for 10 min before data acquisition. Depaking of ^{2}H SS-NMR spectra was conducted using MATLAB with the dePaking script published and provided by the Brown group at the University of Arizona [11,12]. The dePaked NMR spectra were calculated to represent lipids such that the membrane normal is oriented parallel to the static magnetic field [32]. The dePaked peak picking and quadrupolar splitting values were determined by plotting the dePaked spectra using Igor Pro. The quadrupolar splitting of each doublet pair corresponds to the deuterium atoms bonded to a different carbon on the lipid acyl chain. The peak of the three ^{2}H nuclei bound to the terminal methyl carbon appear as the doublet closest to 0 kHz and is assigned as carbon number 14. The remaining carbon number assignments were made in decreasing order as the quadrupolar splitting values for the respective ^{2}H atoms increased. The quadrupolar splitting for the ^{2}H atoms on the carbons closest to the glycerol backbone appear as a plateau and were estimated by integrating the last broad peak [33]. Order parameters for ^{2}H atoms on each carbon were calculated using the quadrupolar splitting values and the following equation [34],

$$\Delta\nu_Q = \frac{3}{4}\left(\frac{e^2qQ}{h}\right)\cdot S_{CD}, \quad (1)$$

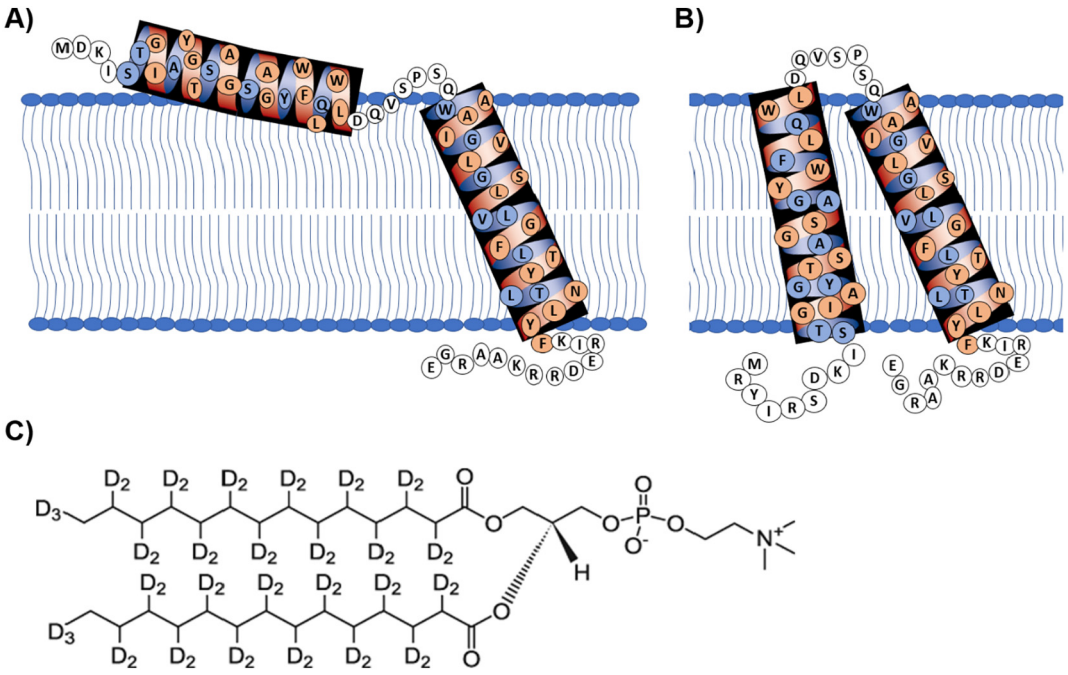

Fig. 1. A) The currently proposed model of the active $S^{21}68$ pinholin with TMD1 partially externalized from the membrane [36]. B) The inactive S^{21}IRS with the additional 5 amino acids seen on the N-terminus of the protein. C) Chemical structure of deuterated DMPC-d_{54} lipid.

where $\Delta\nu_Q$ is the quadrupolar splitting value, $\left(e^2qQ/h\right)$ is the deuterium quadrupolar coupling constant which is equal to 167 kHz for all C-D covalent bonds [35], and S_{CD} is the order parameter for the deuterium on the given carbon.

3. Results and discussion

Previous pinholin research by the Lorigan group showed the successful synthesis, purification, and incorporation of pinholin into membrane mimetic systems [28,36]. The current work utilizes ^{31}P and ^{2}H SS-NMR to investigate the effects of the active $S^{21}68$ and inactive S^{21}IRS pinholin on the dynamic properties of the phospholipid bilayer. The lipid headgroups and acyl chains of DMPC-d_{54} multi lamellar vesicles (MLVs) were studied using ^{31}P chemical shift anisotropy (CSA) and ^{2}H quadrupolar splitting ($\Delta\nu_Q$), respectively. Fig. 1A and B show a schematic representation of the active and inactive forms of pinholin within the membrane while the chemical structure of d_{54}-DMPC can be seen in Fig. 1C [10,28,36,37].

3.1. ^{31}P SS-NMR CSA analysis for the active and inactive forms of pinholin

To investigate the interactions of the active $S^{21}68$ and inactive S^{21}IRS forms of pinholin with the headgroups of the DMPC membrane ^{31}P SS-NMR static spectra were taken at increasing protein concentrations (0–2 mol%). The ^{31}P NMR static spectra at varying mol% for active $S^{21}68$ pinholin are shown in Fig. 2 with increasing temperatures from 25 °C to 55 °C at 10 °C intervals.

All motionally averaged ^{31}P powder-patter spectra are characteristic of axially symmetric ($\sigma_{11} \cong \sigma_{22} \neq \sigma_{33}$) phospholipid bilayers, in this case multi lamellar vesicles, in the liquid crystalline phase (L_α) for all mol% and temperature variants. The chemical shift anisotropy (CSA) for each spectrum was calculated by measuring the difference between σ_{11} ($\sigma_{11} \cong \sigma_{22}$) and σ_{33} of the spectra with all ^{31}P CSA values in the range of 49.3–35.3 ppm (Table 1) [38,39].

For both the 1 and 2 mol% cases of active $S^{21}68$ and inactive S^{21}IRS, the ^{31}P CSA span decreases as the temperature increases. CSA for the active $S^{21}68$ decreased from 45.2 ppm at 25 °C to 42.6 at 55 °C for 1 mol % and from 40.7 ppm to 35.3 ppm for 2 mol% over the same temperature range. The inactive S^{21}IRS pinholin showed a similar inverse trend between temperature and ^{31}P CSA span with the 1 mol% inactive decreasing from 46.6 ppm at 25 °C to 43.3 ppm at 55 °C and 2 mol% decreasing from 44.2 ppm to 39.1 ppm over the same temperature range (Fig. 3).

A comparison of the ^{31}P CSA span between 0, 1, and 2 mol% $S^{21}68$ and S^{21}IRS pinholin is shown in Fig. 4. All data presented in Fig. 4 was collected at 35 °C to ensure the DMPC proteoliposomes are in the liquid crystalline phase. The ^{31}P CSA span is observed to decrease as the mol% of the protein increases for both the active and inactive pinholin. At 35 °C the 0 mol% MLVs have a CSA of 47.3 ppm, the active $S^{21}68$ CSA decreased from 44.5 ppm to 38.4 ppm, while the inactive S^{21}IRS decreased from 46.0 ppm to 43.7 ppm. The overall ^{31}P CSA span comparison between active $S^{21}68$ and inactive S^{21}IRS at 1 and 2 mol% at each temperature reveals in each case that the active $S^{21}68$ pinholin has a lower CSA span value than the inactive S^{21}IRS indicating a higher degree of interaction with the lipid headgroup, when compared to the inactive S^{21}IRS. This trend would be consistent with a partially externalized TMD1 of the active pinholin form laying on the surface of the membrane while TMD1 from the inactive form is still incorporated within the membrane.

Additionally, each spectrum in Figs. 2 and 3 show the presence of an isotropic peak near 0 ppm. This peak in the ^{31}P NMR static spectra is indicative of the fast-relative motion or reorientation of the phospholipid headgroup of DMPC with respect to the ^{31}P NMR timescale. This peak can appear from the presence of lipids tumbling quickly in solution, from lateral diffusion of the lipid, or displacement of lipids over the surface of the membrane [38,40]. The isotropic linewidth for active and inactive pinholin varies from 1.3 ppm for the 1 mol% active $S^{21}68$ at 25 °C to 8.0 ppm for 2 mol% active $S^{21}68$ at 55 °C. A similar trend to that of the CSA can be seen for the isotropic component of active $S^{21}68$ and inactive S^{21}IRS pinholin. For each temperature, as the concentration of the protein increases from 1 to 2 mol% the magnitude and width of the isotropic peak also increases indicating a greater perturbation of the membrane lipid head groups. Just like in the ^{31}P CSA span analysis the active $S^{21}68$ pinholin shows a greater increase of the isotropic peak magnitude and width when compared to that of the inactive S^{21}IRS pinholin. This would be consistent with the overall function of the

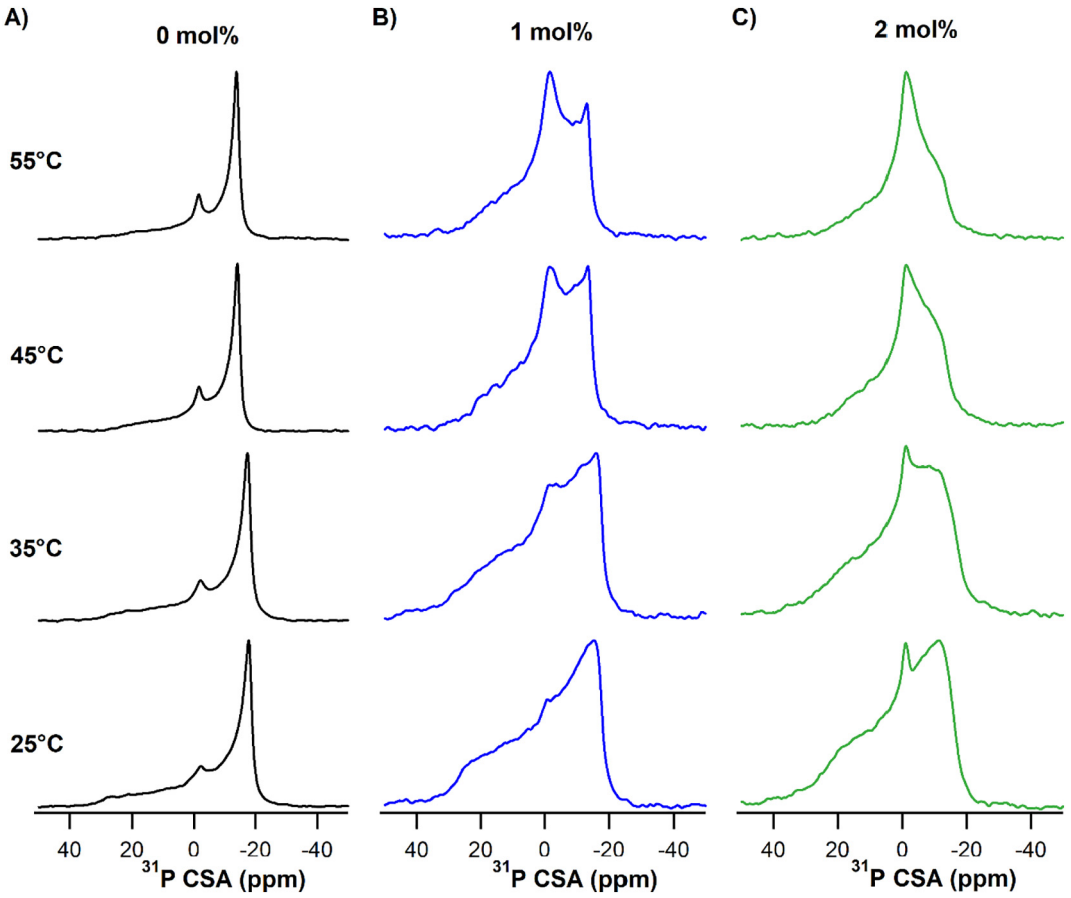

Fig. 2. Temperature dependent ^{31}P SS-NMR spectra of empty d_{54}-DMPC MLVs (A), 1 mol% active S^{21}68 pinholin (B), and 2 mol% active S^{21}68 pinholin (C).

Table 1
The ^{31}P NMR chemical shift anisotropy span (± 0.5 ppm) of empty 0 mol% MLVs, Active S^{21}68 pinholin and inactive S^{21}IRS pinholin at 1 and 2 mol%.

	^{2}H Quad. Splitting (kHz)			
	25 °C	35 °C	45 °C	55 °C
0 mol%	29.8	26.5	24.2	22.6
1 mol% S^{21}68	29.3	25.6	23.4	21.6
2 mol% S^{21}68	28.5	23.6	20.5	19.8
1 mol% S^{21}IRS	28.9	24.9	22.9	21.1
2 mol% S^{21}IRS	27.9	22.9	20.0	19.2

active pinholin as it is a membrane lysing protein. The observed trends of the isotropic peak are indicative of the pinholin's disruption of the lipid bilayer or displacement of the lipids in the bilayer from the partial externalization of TMD1.

3.2. ^{2}H SS-NMR quadrupolar splitting for the active and inactive forms of pinholin

The effect of active and inactive pinholin on the acyl chain dynamics and overall order within the DMPC bilayer were studied using ^{2}H SS-NMR and measuring the corresponding quadrupolar splittings ($\Delta\nu_Q$) and order parameters (S_{CD}). The ^{2}H NMR spectra of 0, 1, and 2 mol% active pinholin incorporated into DMPC-d_{54} MLVs at varying temperatures are shown in Fig. 5.

The ^{2}H NMR spectra shown in Fig. 5 are characteristic of axially symmetric motions for the phospholipids about the membrane normal. The overall ^{2}H NMR spectra are composed of a series of overlaying doublet resonances originating from the twelve different CD_2 positions of DMPC with the highest intensity central doublet corresponding to the terminal CD_3 methyl group of the acyl chain [41,42]. The ^{2}H quadrupole splitting spectral width for the empty MLVs, active, and inactive pinholin at 1 and 2 mol% can be seen in Table 2 and range from 29.8–19.2 kHz. The ^{2}H quadrupole splitting spectral width is a measure of the fluidity of the lipid bilayer [20,41,42].

The decrease in the spectral width of the ^{2}H NMR spectra indicates that the presence of both active S^{21}68 and inactive S^{21}IRS pinholin transmembrane domains disorders the lipid acyl chains for allpeptide/lipid concentrations. This suggests the presence of both active S^{21}68 and inactive S^{21}IRS pinholin transmembrane domain interactions with the acyl chains of the DMPC MLVs. This result is consistent with previously published ^{2}H NMR studies on phospholamban (PLB), since some portion of both active S^{21}68 and inactive S^{21}IRS pinholins have interactions in the headgroup region that increase area per lipid give rise to reduced acyl chain quadrupole splitting [20]. The spectral width for the active S^{21}68 pinholin ranged from 29.3 kHz at 25 °C to 21.6 kHz at 55 °C for 1 mol%, while the spectra for the 2 mol% decreased from 28.5 kHz to 19.8 kHz over the same temperature range. The inactive S^{21}IRS sample showed a similar temperature trend between the spectral widths as the 1 mol% inactive S^{21}IRS decreased from 28.9 kHz at 25 °C to 21.1 kHz at 55 °C while the 2 mol% ranged from 27.9 kHz to 19.2 kHz over the same temperatures. A comparison of the spectral width as active S^{21}68 and inactive S^{21}IRS pinholin concentrations are increased from 1 to 2 mol% at 35 °C is shown in Fig. 6. Active S^{21}68 and inactive S^{21}IRS pinholin both show a decrease in the spectral width as the concentration of the protein increases from 1 to 2 mol%. Unlike in the ^{31}P CSA analysis, the inactive S^{21}IRS shows a greater decrease in the spectral width when compared to that of the active S^{21}68 at the same concentration and temperature.

Additionally, a loss of spectral resolution is apparent in Figs. 5 and 6

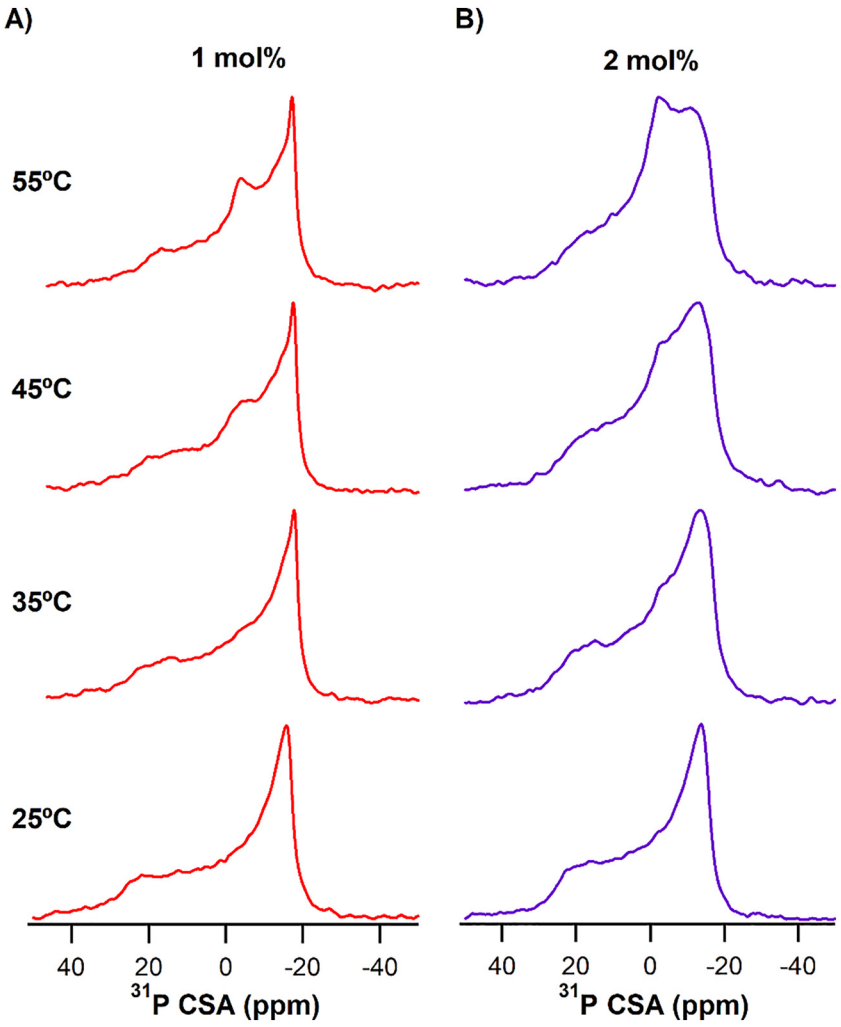

Fig. 3. A) Temperature dependent ^{31}P NMR spectra of d54-DMPC MLVs containing 1 mol% inactive S^{21}IRS pinholin and B) 2 mol% inactive S^{21}IRS pinholin.

as the concentration of pinholin increases, as seen by the absence of the individual sharp doublet peaks throughout each ^{2}H NMR spectrum. The loss in the resolution of each ^{2}H spectrum along with the changes in overall spectral width, is a result of the interactions of the active S^{21}68 and inactive S^{21}IRS pinholin packing against the acyl chains of the lipid bilayer [21,43,44]. A loss of resolution of the ^{2}H NMR spectra shows intermediate-timescale motions of the lipids induced by both active S^{21}68 and inactive S^{21}IRS pinholin. This motion slows the reorientation of the order of the lipid chain [20,21].

The comparison of 1 mol% active S^{21}68 and 1 mol% inactive S^{21}IRS seen in Fig. 6 shows a greater loss in the peak resolution for the inactive form of pinholin, when compared to the active pinholin at the same concentration. This suggests a stronger interaction of the inactive S^{21}IRS pinholin with the acyl chains of the lipid bilayer when compared to that of the pinholin in the active conformation. The greater loss of resolution seen in the 1 mol% inactive S^{21}IRS would indicate a greater number of TMDs present within the bilayer. This is consistent with trends obtained in the quadrupolar splitting analysis and provides further evidence towards the externalization of active S^{21}68 pinholin TMD1 from the membrane yielding fewer acyl chain interactions when compared to inactive S^{21}IRS pinholin.

Fig. 5 also shows an appearance of an isotropic peak centered

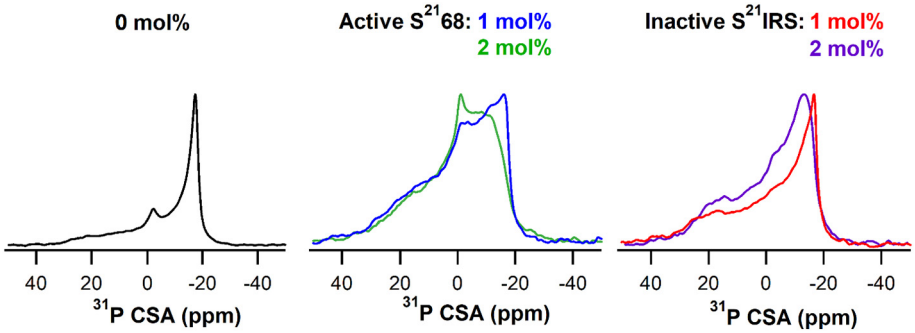

Fig. 4. Comparison of ^{31}P chemical shift anisotropy (CSA) NMR data at 35 °C between empty DMPC-d_{54} MLVs, active S^{21}68, and inactive S^{21}IRS pinholin for 1 and 2 mol% pinholin.

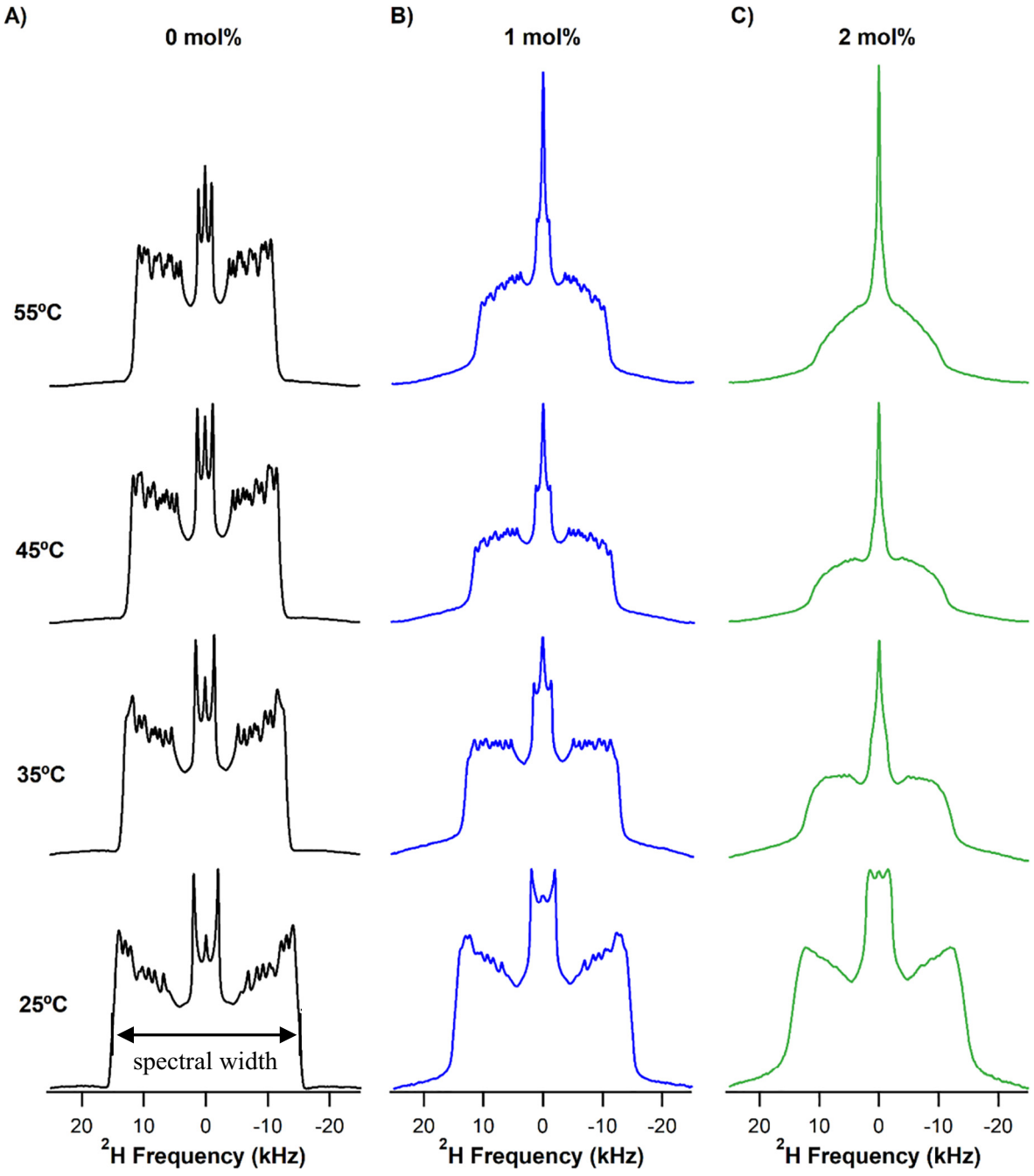

Fig. 5. Temperature dependent ^{2}H SS-NMR spectra of empty DMPC-d_{54} MLVs (A), 1 mol% active S^{21}68 pinholin (B), and 2 mol% active S^{21}68 pinholin (C).

Table 2
The ^{2}H quadrupolar splitting spectral width analysis of empty d54-DMPC MLVs, active S^{21}68, and inactive S^{21}IRS pinholin at 1 and 2 mol% for increasing temperatures. The error in these measurements are ± 0.1–0.3 kHz. These errors were determined by comparing the data from multiple samples.

	^{2}H Quad. Splitting (kHz)			
	25 °C	35 °C	45 °C	55 °C
0 mol%	29.8	26.5	24.2	22.6
1 mol% S^{21}68	29.3	25.6	23.4	21.6
2 mol% S^{21}68	28.5	23.6	20.5	19.8
1 mol% S^{21}IRS	28.9	24.9	22.9	21.1
2 mol% S^{21}IRS	27.9	22.9	22.0	19.2

around 0 kHz which increases as the concentration of active S^{21}68 pinholin increases. This isotropic component is indicative of the fragmentation of the larger MLVs into small sized vesicles which have a fast-relative motion with respect to the NMR timescale. The trends observed in Fig. 5 show a direct correlation between the intensity of the isotropic component and the concentration of active S^{21}68 pinholin in the DMPC bilayers. These results are consistent with the ^{31}P SS-NMR data which both show an increase in the isotropic component as a function of the concentration of pinholin but show a higher degree of membrane disruption for active S^{21}68 when compared to that of the inactive S^{21}IRS pinholin.

3.3. Depaking and order parameters (S_{CD})

In order to further explore the dynamic interactions of the active

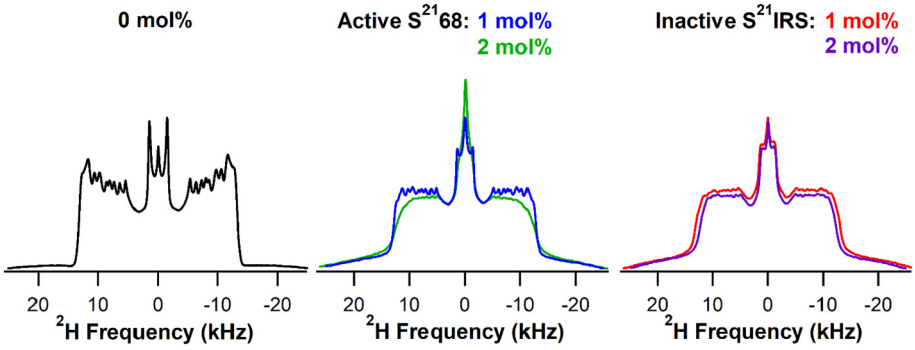

Fig. 6. Comparison of the ^{2}H quadrupolar splitting at 35 °C between empty DMPC-d_{54} liposomes, active S^{21}68, and inactive S^{21}IRS pinholin at 1 and 2 mol% pinholin.

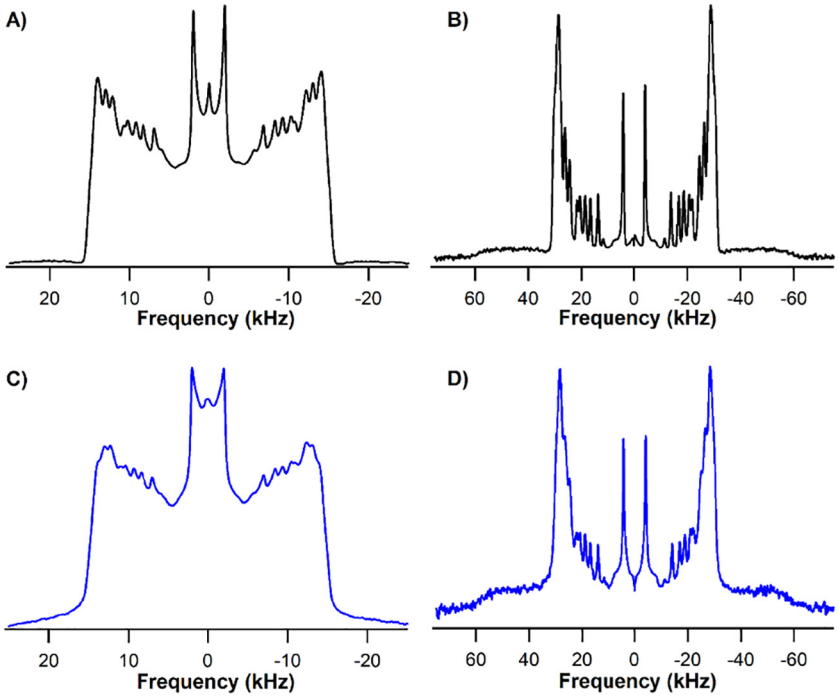

Fig. 7. (A) The original ^{2}H SS-NMR spectra of empty 0 mol% MLVs at 25 °C. (B) The resulting dePaked spectra for empty 0 mol% MLVs. (C and D) The original ^{2}H SS-NMR spectra of 1 mol% active S^{21}68 pinholin at 25 °C and the resulting dePaked spectra, respectively.

and inactive forms of pinholin with the phospholipid bilayer, order parameters (S_{CD}) were calculated from the ^{2}H SS-NMR data. The packing of DMPC acyl chains or order parameters defines the dynamic perturbations or local packing of each individual C–D bond of the standard DMPC acyl chain conformations as the concentration of active and inactive pinholin increases within the bilayer. These order parameters were calculated using Eq. (1) where the quadrupolar splitting values were determined through dePaking of the original ^{2}H SS-NMR spectra shown in Fig. 5. Due to the nature of calculating order parameters large changes in the quadrupolar splitting of peaks in the dePaked spectra results in small shifts in the order parameter plot. An illustrative example of dePaking for empty 0 mol% MLVs and 1 mol% active S^{21}68 is seen in Fig. 7 and shows the original and dePaked spectra for both cases.

While the decrease in spectral width and increase in the isotropic component are consistent with expected trends, the order parameters for both 2 mol% active S^{21}68 pinholin and 1 mol% inactive S^{21}IRS pinholin could not be calculated due to the loss in resolution of the original spectra that was discussed in the previous section. The dePaked spectra for all active S^{21}68 samples can be seen in Supplemental Fig. S1. Order parameter values ranged from the most disordered, 0.015 for the CD_3 terminal methyl, to the most ordered, 0.23 for the CD_2 closest to the glycerol backbone, all of which are characteristic values of DMPC bilayers in the liquid-crystalline phase. The trends of the order parameters at varying temperatures for empty 0 mol% MLVs and 1 mol% active S^{21}68 pinholin show a decrease in the overall order of the system as the temperature increases. The overall decrease in order parameters for each CD_2 moving further away from the glycerol backbone can be seen in Fig. 8 for both 0 mol% and 1 mol% active S^{21}68 at all temperatures.

The effect of temperature on this profile is characteristic of an increase in mobility, or decrease in order, of the acyl chains both of which would be true of a system at higher temperatures [45]. To better see the differences between order parameters an overlaid comparison of the order parameters between 0 mol% and 1 mol% active S^{21}68 pinholin at 35 °C can be seen in Fig. 9. A greater separation between the order parameters of the carbons near the glycerol backbone indicate more disorder in the presence of 1 mol% active S^{21}68. The overlaid dePaked spectra used to find quadrupolar splitting values of 0 mol% and 1 mol% active S^{21}68 at 35 °C can be seen in the Supplementary Information (Fig. S2) which highlights the shift observed for each peak throughout the acyl chain. The trends observed in Fig. 9 are consistent with all the

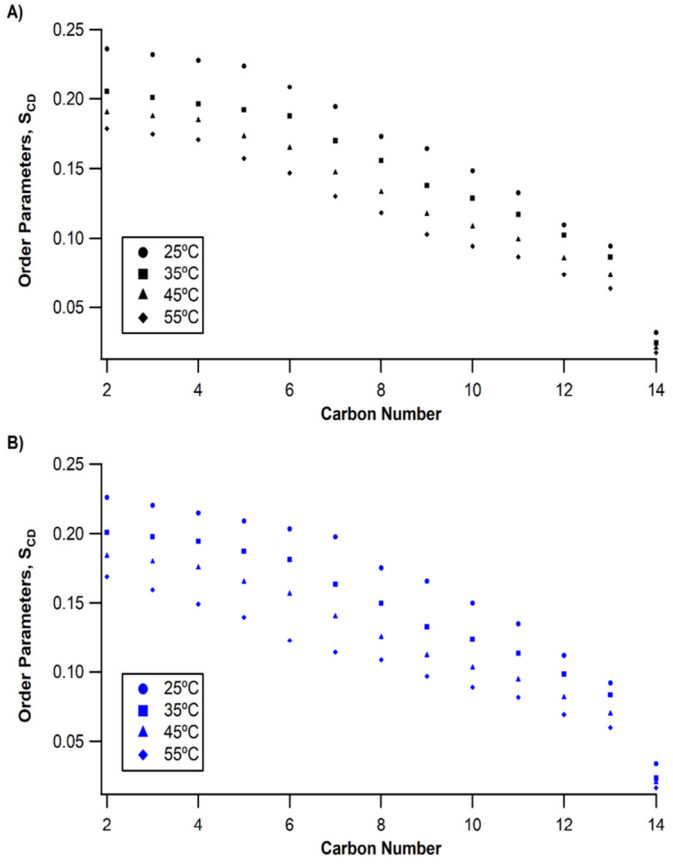

Fig. 8. A) Order parameters (S_{CD}) for 0 mol% MLVs at increasing temperatures. B) Order parameters (S_{CD}) for 1 mol% active $S^{21}68$ pinholin at increasing temperatures. The error in these measurements are ± 0.005. These errors were determined by comparing the data from multiples samples.

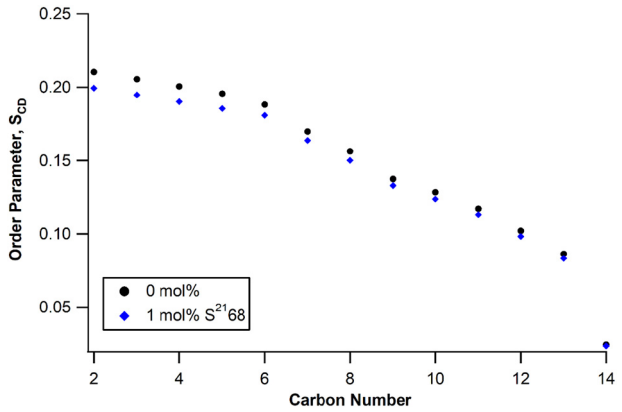

Fig. 9. Order parameter (S_{CD}) comparison at 35 °C between empty 0 mol% MLVs (black) and 1 mol% active $S^{21}68$ pinholin (blue). The error in these measurements are ± 0.001. These errors were determined by comparing the data from multiple sample preparations.

previous data shown and support the partial externalization of active $S^{21}68$ TMD1 from the membrane as the helix interacts with the carbons closest to the membrane surface. The interaction of the externalized TMD1 of the active $S^{21}68$ with lipid headgroups may induce an increase in area per lipid that might give a change in the order parameter profile as shown in Fig. 9. The changes in the order parameters at the membrane core also might be consequences of interactions in the head group region that alter the area per lipid density. Thus, changing the capacity of the core to accommodate acyl chain reorientation.

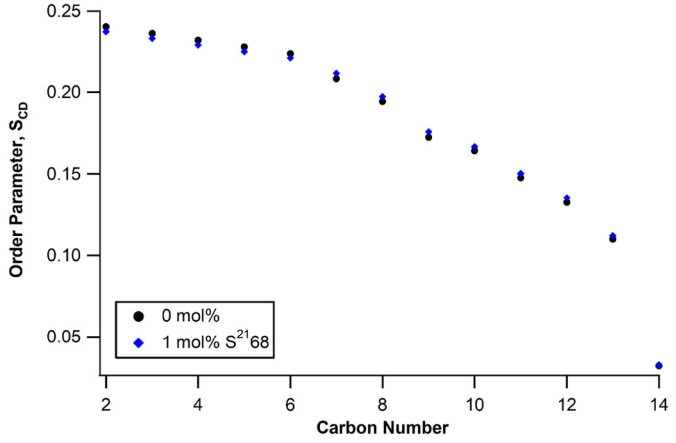

Fig. 10. Order parameter (S_{CD}) comparison at 25 °C between empty 0 mol% MLVs (black) and 1 mol% active $S^{21}68$ pinholin (blue). The order parameters below carbon-7 for 1 mol% active $S^{21}68$ show more order than the 0 mol% sample to compensate for the positive hydrophobic mismatch of the bilayer. The error in these measurements are ± 0.0005. These errors were determined by comparing data from multiple samples.

Alternatively, an interesting trend was observed for the order parameters of active $S^{21}68$ pinholin near the phase transition (25 °C) of the DMPC bilayer. A comparison of the order parameters between 0 mol % and 1 mol% active $S^{21}68$ pinholin at 25 °C can be seen in Fig. 10. This shows more disorder for the carbons closer to the glycerol backbone in the presence of 1 mol% active $S^{21}68$. The overlaid dePaked spectra used to find quadrupolar splitting values of 0 mol% and 1 mol% active $S^{21}68$ at 25 °C can be seen in the Supplementary Information (Fig. S3) which highlights the shifts observed for each peak throughout the acyl chain. Interestingly, at temperatures near the phase transition of DMPC the order parameters below carbon-7 indicate a more ordered environment in the presence of active $S^{21}68$ pinholin when compared to the empty DMPC liposomes. This is due to the lipid compensation for a positive hydrophobic mismatch occurring in the DMPC bilayer.

For a typical alpha helix each helical turn comprises of 3.6 amino acids, correlating to each amino acid contributing 1.5 Å to the helix length. This indicates the TMDs of pinholin are both > 33 Å in length. The average hydrophobic thickness for a DMPC bilayer is ~25 Å. This results in residues of the helix intended to be located within the lipid bilayer instead residing outside of the membrane bilayer. This is known as a positive hydrophobic mismatch [46–48]. This mismatch can be resolved through an ordering of the acyl chains packing around the transmembrane helix resulting in an increase in the local hydrophobic thickness of the bilayer [46,47]. In this case, the higher order parameters seen below carbon-7 in Fig. 10 would be indicative of this higher degree of ordering of the acyl chains. Other possible contribution is that this mismatch can be resolved through introducing a helical tilt of 34° as suggested by a previous study from the Young group [37]. Future studies could be conducted using longer chained lipids to avoid the presence of this mismatch at lower temperatures.

4. Conclusion

Utilizing ^{31}P and ^{2}H SS-NMR spectroscopy, this study compares the interactions of phospholipid bilayers with the active $S^{21}68$ and inactive $S^{21}IRS$ forms of pinholin. ^{31}P SS-NMR nuclei were used to probe the interaction of pinholin with the lipid headgroups. The ^{31}P CSA width values of 1 and 2 mol% active $S^{21}68$ are smaller than the inactive $S^{21}IRS$ CSA values at the same mol% and temperature. The decrease in CSA indicates a higher degree of perturbations at the surface of the membrane for the active $S^{21}68$ pinholin than the inactive $S^{21}IRS$ form of pinholin. This is consistent with the previously proposed model of TMD1 partially externalizing from the lipid bilayer. The ^{31}P SS-NMR

spectra also show an isotropic peak with an increasing magnitude and width as the concentration of pinholin increases. A greater linewidth for the active over the inactive pinholin could be a result of displacement of the lipids in the bilayer coming from the partial externalization of TMD1 or possibly due to the lysing function of the active $S^{21}68$ pinholin which would induce a greater amount of disruption of the lipid bilayer.

The ^{2}H SS-NMR quadrupolar splitting data showed an overall decrease in the spectral width as the mol% of pinholin increased. Unlike ^{31}P CSA trends, the inactive $S^{21}IRS$ showed a greater decrease in the ^{2}H quadrupolar splitting. This trend indicates a greater degree of interaction with the acyl chains of the lipid coming from the inactive form of the pinholin. These interactions are originating from the presence of TMD1 remaining within the membrane for the inactive form of the pinholin. This is further supported by the additional loss in resolution of the doublet peaks observed when comparing 1 mol% inactive $S^{21}IRS$ to the spectra for 1 mol% active $S^{21}68$ pinholin. The order parameters determined from the quadrupolar splitting of the dePaked ^{2}H spectra give further support for the conclusions drawn from the ^{31}P and ^{2}H data. The decrease in the order parameters of carbon 2–6 in the presence of 1 mol% active $S^{21}68$ pinholin support the idea of a partial TMD1 externalization from the membrane. This study also highlights the application of SS-NMR spectroscopy to distinguish between the two different conformations of the pinholin protein and the resulting interactions with the lipid bilayer.

Transparency document

The Transparency document associated with this article can be found, in online version.

Acknowledgements

We would like to thank Dr. Theresa Ramelot for her continuous support for the solid-state NMR instruments and data processing. The MATLAB software code used to dePake our ^{2}H spectrum was kindly provided by the Brown group at University of Arizona. We are also grateful to the members of the Young group at Texas A&M University for their experimental suggestions. This work was generously supported by a NSF CHE-1807131 grant and a NIGMS/NIH Maximizing Investigator's Research Award (MIRA) R35 GM126935 award. Gary A. Lorigan would also like to acknowledge support from the John W. Steube Professorship.

Appendix A. Supplementary data

Supplementary data to this article can be found online at https://doi.org/10.1016/j.bbamem.2020.183257.

References

[1] R. Young, Phage lysis: do we have the hole story yet? Curr. Opin. Microbiol. 16 (2013) 1–8.
[2] R. Young, Phage lysis: three steps, three choices, one outcome, J. Microbiol. 52 (2014) 243–258, https://doi.org/10.1007/s12275-014-4087-z.
[3] K.H. To, R. Young, Probing the structure of the S105 hole, J. Bacteriol. 196 (2014) 3683–3689, https://doi.org/10.1128/jb.01673-14.
[4] J.S. Dewey, C.G. Savva, R.L. White, S. Vitha, A. Holzenburg, R. Young, Micron-scale holes terminate the phage infection cycle, Proc. Natl. Acad. Sci. U. S. A. 107 (2010) 2219–2223, https://doi.org/10.1073/pnas.0914030107.
[5] I.N. Wang, J. Deaton, R. Young, Sizing the holin lesion with an endolysin-beta-galactosidase fusion, J. Bacteriol. 185 (2003) 779–787, https://doi.org/10.1128/jb.185.3.779-787.2003.
[6] T. Park, D.K. Struck, C.A. Dankenbring, R. Young, The pinholin of lambdoid phage 21: control of lysis by membrane depolarization, J. Bacteriol. 189 (2007) 9135–9139, https://doi.org/10.1128/jb.00847-07.
[7] M. Barenboim, C.Y. Chang, F.D. Hajj, R. Young, Characterization of the dual start motif of a class II holin gene, Mol. Microbiol. 32 (1999) 715–727, https://doi.org/10.1046/j.1365-2958.1999.01385.x.
[8] M.T. Bonovich, R. Young, Dual start motif in 2 lambdoid s-genes unrelated to lambda-s, J. Bacteriol. 173 (1991) 2897–2905.
[9] T. Pang, T. Park, R. Young, Mapping the pinhole formation pathway of S21, Mol. Microbiol. 78 (2010) 710–719, https://doi.org/10.1111/j.1365-2958.2010.07362.x.
[10] T. Park, D.K. Struck, J.F. Deaton, R. Young, Topological dynamics of holins in programmed bacterial lysis, Proc. Natl. Acad. Sci. U. S. A. 103 (2006) 19713–19718, https://doi.org/10.1073/pnas.0600943103.
[11] J.J. Kinnun, A. Leftin, M.F. Brown, Solid-state NMR spectroscopy for the physical chemistry laboratory, J. Chem. Educ. 90 (2013) 123–128, https://doi.org/10.1021/ed2004774.
[12] T.R. Molugu, S. Lee, M.F. Brown, Concepts and methods of solid-state NMR spectroscopy applied to biomembranes, Chem. Rev. 117 (2017) 12087–12132, https://doi.org/10.1021/acs.chemrev.6b00619.
[13] A. Arora, L.K. Tamm, Biophysical approaches to membrane protein structure determination, Curr. Opin. Struct. Biol. 11 (2001) 540–547, https://doi.org/10.1016/s0959-440x(00)00246-3.
[14] C.E. Dempsey, N.J.P. Ryba, A. Watts, Evidence from deuterium nuclear-magnetic-resonance for the temperature-dependent reversible self-association of erythrocyte band-3 in dimyristoylphosphatidylcholine bilayers, Biochemistry 25 (1986) 2180–2187, https://doi.org/10.1021/bi00356a049.
[15] M.A. Lemmon, D.M. Engelman, Specificity and promiscuity in membrane helix interactions, FEBS Lett. 346 (1994) 17–20, https://doi.org/10.1016/0014-5793(94)00467-6.
[16] A. Watts, Protein-lipid interactions - do the spectroscopists now agree, Nature 294 (1981) 512–513, https://doi.org/10.1038/294512a0.
[17] M.R. Morrow, C.W.M. Grant, The EGF receptor transmembrane domain: peptide-peptide interactions in fluid bilayer membranes, Biophys. J. 79 (2000) 2024–2032, https://doi.org/10.1016/s0006-3495(00)76450-2.
[18] A.C. Rigby, K.R. Barber, G.S. Shaw, C.W.M. Grant, Transmembrane region of the epidermal growth factor receptor: behavior and interactions via H-2 NMR, Biochemistry 35 (1996) 12591–12601, https://doi.org/10.1021/bi9611063.
[19] S. Sharpe, K.R. Barber, C.W.M. Grant, D. Goodyear, M.R. Morrow, Organization of model helical peptides in lipid bilayers: insight into the behavior of single-span protein transmembrane domains, Biophys. J. 83 (2002) 345–358, https://doi.org/10.1016/s0006-3495(02)75174-6.
[20] P.C. Dave, E.K. Tiburu, K. Damodaran, G.A. Lorigan, Investigating structural changes in the lipid bilayer upon insertion of the transmembrane domain of the membrane-bound protein phospholamban utilizing P-31 and H-2 solid-state NMR spectroscopy, Biophys. J. 86 (2004) 1564–1573.
[21] S. Abu-Baker, G.A. Lorigan, Phospholamban and its phosphorylated form interact differently with lipid bilayers: a (31)P, (2)H, and (13)C solid-state NMR spectroscopic study, Biochemistry 45 (2006) 13312–13322, https://doi.org/10.1021/bi0614028.
[22] J.S. Santos, D.K. Lee, A. Ramamoorthy, Effects of antidepressants on the conformation of phospholipid headgroups studied by solid-state NMR, Magn. Reson. Chem. 42 (2004) 105–114, https://doi.org/10.1002/mrc.1327.
[23] B.W. Koenig, J.A. Ferretti, K. Gawrisch, Site-specific deuterium order parameters and membrane-bound behavior of a peptide fragment from the intracellular domain of HIV-1 gp41, Biochemistry 38 (1999) 6327–6334, https://doi.org/10.1021/bi982800g.
[24] S. Yamaguchi, D. Huster, A. Waring, R.I. Lehrer, W. Kearney, B.F. Tack, M. Hong, Orientation and dynamics of an antimicrobial peptide in the lipid bilayer by solid-state NMR spectroscopy, Biophys. J. 81 (2001) 2203–2214, https://doi.org/10.1016/s0006-3495(01)75868-7.
[25] P.R. Hansen, A. Oddo, Fmoc solid-phase peptide synthesis, Peptide Antibodies: Methods and Protocols 1348 (2015) 33–50, https://doi.org/10.1007/978-1-4939-2999-3_5.
[26] P. Lloyd-Williams, F. Albericio, E. Giralt, Chemical Approaches to the Synthesis of Peptides and Proteins, CRC Press, 1997.
[27] D.S. King, C.G. Fields, G.B. Fields, A cleavage method which minimizes side reactions following fmoc solid-phase peptide-synthesis, Int. J. Pept. Protein Res. 36 (1990) 255–266.
[28] D.L. Drew, T. Ahammad, R.A. Serafin, B.J. Butcher, K.R. Clowes, Z. Drake, I.D. Sahu, R.M. McCarrick, G.A. Lorigan, Solid phase synthesis and spectroscopic characterization of the active and inactive forms of bacteriophage S-21 pinholin protein, Anal. Biochem. 567 (2019) 14–20, https://doi.org/10.1016/j.ab.2018.12.003.
[29] I.D. Sahu, R.M. McCarrick, G.A. Lorigan, Use of electron paramagnetic resonance to solve biochemical problems, Biochemistry 52 (2013) 5967–5984, https://doi.org/10.1021/bi400834a.
[30] G. Dixit, I.D. Sahu, W.D. Reynolds, T.M. Wadsworth, B.D. Harding, C.K. Jaycox, C. Dabney-Smith, C.R. Sanders, G.A. Lorigan, Probing the dynamics and structural topology of the reconstituted human KCNQ1 voltage sensor domain (Q1-VSD) in lipid bilayers using electron paramagnetic resonance spectroscopy, Biochemistry 58 (2019) 965–973, https://doi.org/10.1021/acs.biochem.8b01042.
[31] J.H. Davis, K.R. Jeffrey, M. Bloom, M.I. Valic, T.P. Higgs, Quadrupolar echo deuteron magnetic-resonance spectroscopy in ordered hydrocarbon chains, Chem. Phys. Lett. 42 (1976) 390–394, https://doi.org/10.1016/0009-2614(76)80392-2.
[32] T.R. Molugu, X. Xu, A. Leftin, S. Lope-Piedraffita, G.V. Martinez, H.I. Petrache, M.F. Brown, Solid-State Deuterium NMR Spectroscopy of Membranes, in: G. Webb (Ed.), Modern Magnetic Resonance, Springer, Cham, 2017, pp. 1–23, , https://doi.org/10.1007/978-3-319-28275-6_89-1.
[33] M. Lafleur, B. Fine, E. Sternin, P.R. Cullis, M. Bloomt, Smoothed orientational order profile of lipid bilayers by 2H-nuclear magnetic resonance, Biophys. J. 56 (1989) 1037–1041.
[34] A. Drechsler, G. Anderluh, R.S. Norton, F. Separovic, Solid-state NMR study of membrane interactions of the pore-forming cytolysin, equinatoxin II, Biochimica Et

Biophysica Acta-Biomembranes 1798 (2010) 244–251, https://doi.org/10.1016/j.bbamem.2009.10.012.
[35] J. Seelig, H.-U. Gally, R. Wohlgemuth, Orientation and flexibility of the choline head group in phosphatidylcholine bilayers, Biochim. Biophys. Acta Biomembr. 467 (1977) 109–119.
[36] T. Ahammad, D.L. Drew Jr., I.D. Sahu, R.A. Serafin, K.R. Clowes, G.A. Lorigan, Continuous wave electron paramagnetic resonance spectroscopy reveals the structural topology and dynamic properties of active pinholin $S2^{16}8$ in a lipid bilayer, J. Phys. Chem. B 123 (2019) 8048–8056.
[37] T. Pang, C.G. Savva, K.G. Fleming, D.K. Struck, R. Young, Structure of the lethal phage pinhole, Proc. Natl. Acad. Sci. U. S. A. 106 (2009) 18966–18971, https://doi.org/10.1073/pnas.0907941106.
[38] J. Seelig, P-31 nuclear magnetic-resonance and head group structure of phospholipids in membranes, Biochim. Biophys. Acta 515 (1978) 105–140, https://doi.org/10.1016/0304-4157(78)90001-1.
[39] A.C. McLaughlin, P.R. Cullis, J.A. Berden, R.E. Richards, P-31 NMR of phospholipid membranes - effects of chemical-shift anisotropy at high magnetic-field strengths, J. Magn. Reson. 20 (1975) 146–165, https://doi.org/10.1016/0022-2364(75)90162-6.
[40] T.L. Lau, E.E. Ambroggio, D.J. Tew, R. Cappai, C.L. Masters, G.D. Fidelio, K.J. Barnham, F. Separovic, Amyloid-beta peptide disruption of lipid membranes and the effect of metal ions, J. Mol. Biol. 356 (2006) 759–770, https://doi.org/10.1016/j.jmb.2005.11.091.
[41] J. Seelig, Deuterium magnetic-resonance - theory and application to lipid-membranes, Q. Rev. Biophys. 10 (1977) 353–418, https://doi.org/10.1017/s0033583500002948.
[42] M. Lafleur, M. Bloom, P.R. Cullis, Lipid polymorphism and hydrocarbon order, Biochemistry and Cell Biology-Biochimie Et Biologie Cellulaire 68 (1990) 1–8, https://doi.org/10.1139/o90-001.
[43] R.E. Minto, P.R. Adhikari, G.A. Lorigan, A H-2 solid-state NMR spectroscopic investigation of biomimetic bicelles containing cholesterol and polyunsaturated phosphatidylcholine, Chem. Phys. Lipids 132 (2004) 55–64, https://doi.org/10.1016/j.chemphyslip.2004.09.005.
[44] D. Huster, Solid-state NMR spectroscopy to study protein lipid interactions, Biochimica Et Biophysica Acta-Molecular and Cell Biology of Lipids 1841 (2014) 1146–1160, https://doi.org/10.1016/j.bbalip.2013.12.002.
[45] H.I. Petrache, S.W. Dodd, M.F. Brown, Area per lipid and acyl length distributions in fluid phosphatidylcholines determined by H-2 NMR spectroscopy, Biophys. J. 79 (2000) 3172–3192, https://doi.org/10.1016/s0006-3495(00)76551-9.
[46] S.K. Kandasamy, R.G. Larson, Molecular dynamics simulations of model transmembrane peptides in lipid bilayers: a systematic investigation of hydrophobic mismatch, Biophys. J. 90 (2006) 2326–2343, https://doi.org/10.1529/biophysj.105.073395.
[47] T. Kim, K.I. Lee, P. Morris, R.W. Pastor, O.S. Andersen, W. Im, Influence of hydrophobic mismatch on structures and dynamics of gramicidin A and lipid bilayers, Biophys. J. 102 (2012) 1551–1560, https://doi.org/10.1016/j.bpj.2012.03.014.
[48] C. Muhle-Goll, S. Hoffmann, S. Afonin, S.L. Grage, A.A. Polyansky, D. Windisch, M. Zeitler, J. Burck, A.S. Ulrich, Hydrophobic matching controls the tilt and stability of the dimeric platelet-derived growth factor receptor (PDGFR) beta transmembrane segment, J. Biol. Chem. 287 (2012) 26178–26186, https://doi.org/10.1074/jbc.M111.325555.